Nuclear Physics A554 (1993) 257–286
North-Holland

NUCLEAR
PHYSICS A

# Dynamical instability and nuclear multifragmentation in BUU model for heavy-ion collisions

Bao-An Li and D.H.E. Gross[1]

*Hahn-Meitner-Institut, Bereich Kern- und Strahlenphysik, Glienickerstrasse 100, W-1000 Berlin 39, Germany*

Received 4 September 1992

**Abstract:** By simulating numerically the reaction dynamics of intermediate-energy heavy-ion collisions within the Boltzmann-Uehling-Uhlenbeck (BUU) transport model, we study systematically the onset of dynamical instabilities and nuclear multifragmentation in central collisions of $^{96}$Mo + $^{96}$Mo at beam energies of 55 and 100 MeV/nucleon. It is found that dynamical instabilities characterized by an imaginary adiabatic sound velocity in the central region of the reaction develop during the expansion phase of the reaction. Thermalization can be reached at about the same time when the dynamical instabilities set in. Multifragmentation patterns, geometries of final-fragment distributions as well as their dependence on the nuclear equation of state and the beam energy are also studied by making scatter plots of the one-body density distributions.

## 1. Introduction

Nuclear multifragmentation characterized by the emission of three or more intermediate-mass fragments with a mass of $A \geq 10$ is a natural continuation of fission towards higher excitation energies [1]). At excitation energies $E^* \approx \frac{3}{4}B$, the binding energy of the nucleus, it is mainly triggered by the competition of the repulsive Coulomb energy against the surface tension very much like nuclear fission at low excitation energies [2]). At substantially higher excitations, $E^* \gg B$, the repulsive long-range Coulomb force is not anymore driving the system towards fragmentation into large pieces. Here the situation is more like the liquid to gas transition in an ordinary neutral, overheated macroscopic drop [3–6]). Expanded nuclear systems at densities and temperatures corresponding to the liquid-gas coexistence region are expected to decay into many intermediate-mass fragments [7,8]).

Besides target fragmentations in proton-induced reactions [9]), now the multifragmentation is frequently found in heavy-ion-induced reactions [e.g. refs. [10–13])]. The phenomenon has been explained in a variety of ways and has been a subject of much debate. Available models can be divided into two groups: static and dynamic models.

Correspondence to: Dr. Bao-An Li, Bereich Kern- und Strahlenphysik, Hahn-Meitner Institut, Glienickerstrasse 100, W-1000 Berlin 39, Germany.

[1] Also at Fachbereich Physik der Freien Universität, Berlin, Germany.

Among the many static models, statistical models [14-17]) have been rather successful in explaining a number of experimental data. Belonging to the same group, percolation-based phase-transition models have also been very successful in reproducing high-energy proton-induced and light-ion-induced multifragmentation data [18,19]). It was found very recently that for $^{129}Xe+^{197}Au$ reactions at $E/A = 50$ MeV, the percolation model predicts a too low multiplicity of intermediate-mass fragments compared to that of the experimental data [20,21]).

A number of dynamical models have been developed with success at different levels. Among the dynamical models, molecular-dynamics-based models [22,23]) have been widely used for studying multifragmentation. Dynamical models of mean-field approach, represented by the Boltzmann/Vlasov/Nordheim-Uehling-Uhlenbeck models (BUU/VUU/BNV) [24,25]) have been used also to study the mechanism of multifragmentation.

In mean-field approaches, the emphasis has been put on either the nucleation or condensation of localized regions of the system or the development of dynamical instabilities due to the small amplitude, long-wavelength density fluctuations [7,8]). In the final state of the reaction, several nucleons can be close to each other in phase space and the one-body field can bind them together to form a cluster. One of the most important conditions for forming clusters in mean-field approaches is for sufficient fluctuations to be generated during the reaction process. To improve the treatment of fluctuations in the BUU model, several methods have been put forward and studied numerically [26-28]). For the same purpose, multifragmentation was also studied in a hybrid model [29]) by coupling the cascade model [30-32]) for the earlier stage of the reaction and the Vlasov model [33]) for the later stage of the reaction.

Multifragmentation of finite nuclei due to the growth of dynamical instabilities has been studied rather extensively in various dynamical approaches. Dynamical instabilities and fragmentation of hot and compressed nuclei was studied in ref. [34]) using the Vlasov-Uehling-Uhlenbeck (VUU) model [35]), in ref. [37]) using a simple isentropic expansion model and in ref. [38]) using a hydrodynamical approach with the Thomas-Fermi approximation. The quasiparticle-dynamics model [39]) has also been used to study the fluctuation growth in finite nuclei. A two-dimensional field model based on a wave mechanical description has been used for the same purpose in ref. [40]). More recently, the Boltzmann-Langevin model [28]) was used to study multifragmentation of a uniform gas initialized at a density and temperature corresponding to the mechanical instability region [41]).

However, multifragmentation in real nucleus-nucleus collisions due to the growth of dynamical instabilities was not studied until very recently [42-44]). By performing the Boltzmann-Nordheim-Vlasov model (BNV) [45]) calculations, Moretto *et al.* observed multifragmentation in central $^{96}Mo+^{96}Mo$ reactions at beam energies from 55 to 100 MeV/nucleon. Stimulated by the strong oblate deformation of the dense part of the system before its fragmentation, they suggested a breaking of the "thin" disk due to Rayleigh-Taylor surface instabilities. Our recent BUU-model calcula-

tions using a soft nuclear equation of state show multifragmentation from a more or less spherical source in central Mo+Mo reactions at a beam energy of 55 MeV/nucleon. Dynamical instabilities characterized by an imaginary adiabatic sound velocity is observed to develop in the expansion phase of the reaction. We have published brief results of this work recently [44]). It is interesting to note that in a recent paper also Bauer used the BUU model to study bubble and ring formation and their subsequent decay by multifragmentation [43]). Their results on central collisions of $^{93}$Nb+$^{93}$Nb at a beam energy of 60 MeV/nucleon show similar fragmentation patterns as ours.

In the present paper we investigate dynamical instabilities and multifragmentation more completely within the BUU model for intermediate-energy heavy-ion collisions. Our aims are twofold. Firstly, we study rather systematically by using different nuclear equations of states and beam energies the development of dynamical instabilities and the corresponding fragmentation patterns. Secondly, since the BUU model is based on a truncated one-body transport theory [46,47]) and therefore lacks information on many-body correlations which are necessary to describe fragments, the fragments seen in the BUU calculations should not be considered literally as realistic fragments. To practically study properties of the fragments and compare with experimental data, we propose to couple the BUU model with a statistical model for multifragmentation, such as that described in ref. [2]). The necessary condition and inputs for the statistical model are the establishment of a more or less thermalized source, the size, mass number, charge number and the excitation energy of the source. We will therefore study the thermalization, size and mass number of the heavy residue in which dynamical instabilities may develop.

The paper is organized as follows. We will first briefly introduce the BUU model and the inputs used in this study in the next section. In sect. 3, we present and discuss results of our calculations. A summary will be given at the end.

## 2. The model

Our study is based on the nuclear Boltzmann-Uehling-Uhlenbeck transport theory [24,25]), where the transport equation for the nucleonic one-body density distribution function $f_1 = f(\boldsymbol{r}_1, \boldsymbol{p}_1, t)$ is given by

$$\partial_t f_1 + \frac{\boldsymbol{p}}{E}\cdot\boldsymbol{\nabla}_r f_1 - \boldsymbol{\nabla}_r U\cdot\boldsymbol{\nabla}_p f_1 \tag{1}$$

$$= \int \frac{\mathrm{d}^3p_1\,\mathrm{d}^3p_2\,\mathrm{d}^3p_{2'}}{(2\pi)^9}\,\sigma v_{12}(2\pi)^3\delta^3(\boldsymbol{p}_1+\boldsymbol{p}_2-\boldsymbol{p}_{1'}-\boldsymbol{p}_{2'})$$

$$\times\{f_1 f_{2'}(1-f_1)(1-f_2)-f_1 f_2(1-f_{1'})(1-f_{2'})\}\,. \tag{2}$$

In our numerical implementation we use the test-particle method [33]), in which the solution of eq. (1) is reduced to the solution of a set of $6\times(A_t+A_p)\times N$ coupled

first-order differential equations in time, where $N$ is the number of test-particles per nucleon, and $A_t$ and $A_p$ are the target and projectile mass numbers, respectively. $N = 150$ is used in the following. The numerical details of the code used in the present study can be found in refs. [48-50]).

The mean-field potential $U$ appearing in eq. (1) is parametrized as a density-dependent functional,

$$U(\rho) = a(\rho/\rho_0) + b(\rho/\rho_0)^{\sigma}. \tag{3}$$

Correspondingly, the potential energy density is given by

$$W(\rho) = \int U(\rho)\,\mathrm{d}\rho = \frac{a}{2}\frac{\rho^2}{\rho_0} + \frac{b}{1+\sigma}\left(\frac{\rho}{\rho_0}\right)^{\sigma}\rho. \tag{4}$$

The parameters $a$, $b$ and $\sigma$ are determined by nuclear-matter saturation properties and the nuclear-matter compressibility coefficient $K$. Here the coefficient $K$ of nuclear matter at normal density is defined as

$$K = 9(\partial P/\partial\rho)_S = 9\left(\frac{p_F^2}{3m} + a + b\sigma\right). \tag{5}$$

where the derivative is taken adiabatically, $P$ is the pressure and $p_F$ is the Fermi momentum. Properties of nuclear matter are still not very well known. Current knowledge comprehends a narrow region around the nuclear ground state, namely, only density $\rho_0 = 0.17\ \mathrm{fm}^{-3}$ and binding energy per nucleon $E/A = -15.75$ MeV, are well determined while even the compressibility coefficient at equilibrium is only known to lie between 210 MeV [ref. [51])] and 310 MeV [ref. [52])]. For high-density and high-temperature nuclear matter no reliable information is available. In the present study we therefore use three different compressibility coefficients $K$ of 200, 380 and 540 MeV to study its effects. The parameters $a$, $b$ and $\sigma$ are given in table 1 for the three different $K$'s.

To see the difference between the three equation of states and their density dependence, we present in fig. 1 the energy per nucleon for nuclear matter at zero temperature,

$$\frac{E}{A} = \frac{W(\rho)}{\rho} + \frac{3}{5}E_F\left(\frac{\rho}{\rho_0}\right)^{2/3}, \tag{6}$$

TABLE 1

Parameters of the nulear equation of state

| $K$ (MeV) | $a$ | $b$ | $\sigma$ |
|---|---|---|---|
| 200 | −358.1 | 304.8 | 1.167 |
| 380 | −123.6 | 70.4 | 2 |
| 540 | −103.22 | 49.96 | 2.77 |

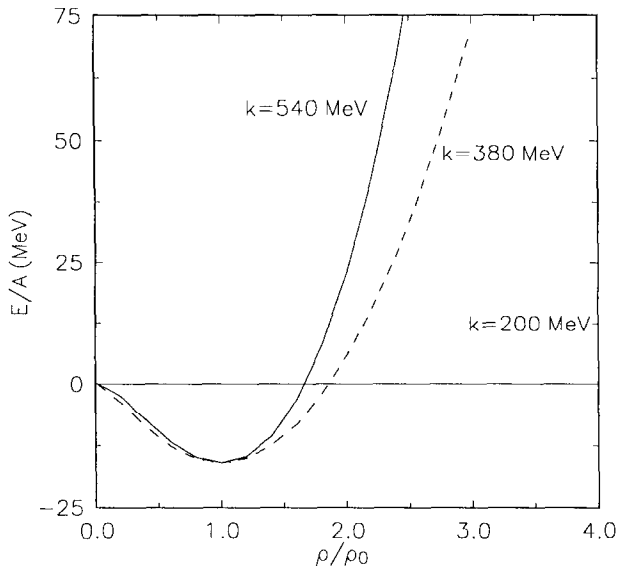


Fig. 1. The nuclear equation of state at zero temperature.

where $E_F = 37.26$ MeV is the Fermi energy. The stiffness of the nuclear equation of state as a function of the compressibility coefficient is obvious.

Within the dynamical instability or spinodal decomposition region, defined by the condition $\partial P/\partial_\rho < 0$ at constant temperature or constant entropy, a homogeneous system is unstable against fluctuation growth and separates into distinct liquid (fragments) and vapor (nucleons) components. We investigate dynamical instabilities and fragmentations with the BUU model both schematically by making scatter plots of one-body densities and quantitatively by studying the adiabatic sound velocity squared,

$$v_s^2 = \frac{1}{m}\left(\frac{\partial P}{\partial \rho}\right)_S . \tag{7}$$

Using the above equation of state and the scaling transformation of the kinetic energy per particle in terms of the nucleon density in the adiabatic expansion process, it can be expressed as [53,43])

$$v_s^2 = \frac{1}{m}\left[\frac{10}{9}\langle E_k\rangle + a\frac{\rho}{\rho_0} + b\sigma\left(\frac{\rho}{\rho_0}\right)^{\alpha}\right], \tag{8}$$

where $\langle E_k\rangle$ is the average kinetic energy per nucleon.

It is worth mentioning that entropy production in heavy-ion collisions has been a subject of many investigations [7,54]), particularly in ref. [22]) molecular-dynamics simulations for hot drops show that the matter almost expands adiabatically until it reaches the region of adiabatic instabilities. In the energy region we studied here,

both the BUU-model and the cascade-model calculations for medium-sized nucleus-nucleus collisions indicate that very little entropy is generated during the expansion phase before the fragmentation occurs [29]). The adiabatic sound velocity can therefore give a good indication of the onset of dynamical instabilities. However, as soon as the sound velocity becomes imaginary the system will run into the entropy-generating period, the adiabatic sound velocity will lose its physical meaning. In ref. [43]) the sound velocity was calculated as a function of time and the distance to the center of mass, it is seen that the dynamical instabilities mainly occur in places close to the center of mass. In the following we will calculate the sound velocity as a function of time for nucleons in a sphere centered at the center of mass with a radius of 2.0 fm.

## 3. Results and discussions

In this section we present and discuss results of our calculations for $^{96}$Mo+$^{96}$Mo reactions at zero impact parameter by using three different nuclear equations of states and two beam energies. We will also study the effect of Coulomb interaction by turning on and off the Coulomb potential.

### 3.1. FRAGMENTATION PATTERNS

To show schematically the development of dynamical instabilities and fragmentation, we show in figs. 2 and 3 scatter plots of $40\times(A_t+A_p)$ test particles out of $150\times(A_t+A_p)$ test particles used in the calculations with and without Coulomb interactions, respectively. The beam energy for the reactions is 55 MeV/nucleon and the compressibility coefficient $K$ is 200 MeV. The reactions are followed upto 300 fm/$c$ since the contact of the two nuclei. We only plotted the $40\times(A_t+A_p)$ test particles in order to compare with results of Moretto *et al.* One can clearly see the onset of fragmentation at about 120 fm/$c$ in both calculations.

The interesting results seen from figs. 2 and 3 can be summarized as the following:

(1) In both calculations, without Coulomb as also with Coulomb, the breaking into fragments occurs when the hot source expanded back to about normal nuclear density. At the moment of breaking, the spatial distribution, especially in the calculation with Coulomb interaction is quite spherical. The fragmentation is clearly over the whole volume. Later, at 120 fm/$c$ in the case without Coulomb a doughnut shape seems to develop, however, we should not emphasize this too much as we know that BUU did become unstable much earlier.

(2) The most interesting result is shown in fig. 4: Here we have plotted the radius of the dense part in the scatter plot of figs. 2 and 3 as a function of time. Here the radius is determined optically by measuring the distance of the outer edge of the dense parts of the scatter plots in the $xy$ plane from the center of mass, since the usually used critical local-density or binding-energy criterion is not appropriate to apply here. In case of existing several fragments, we take the average distance of

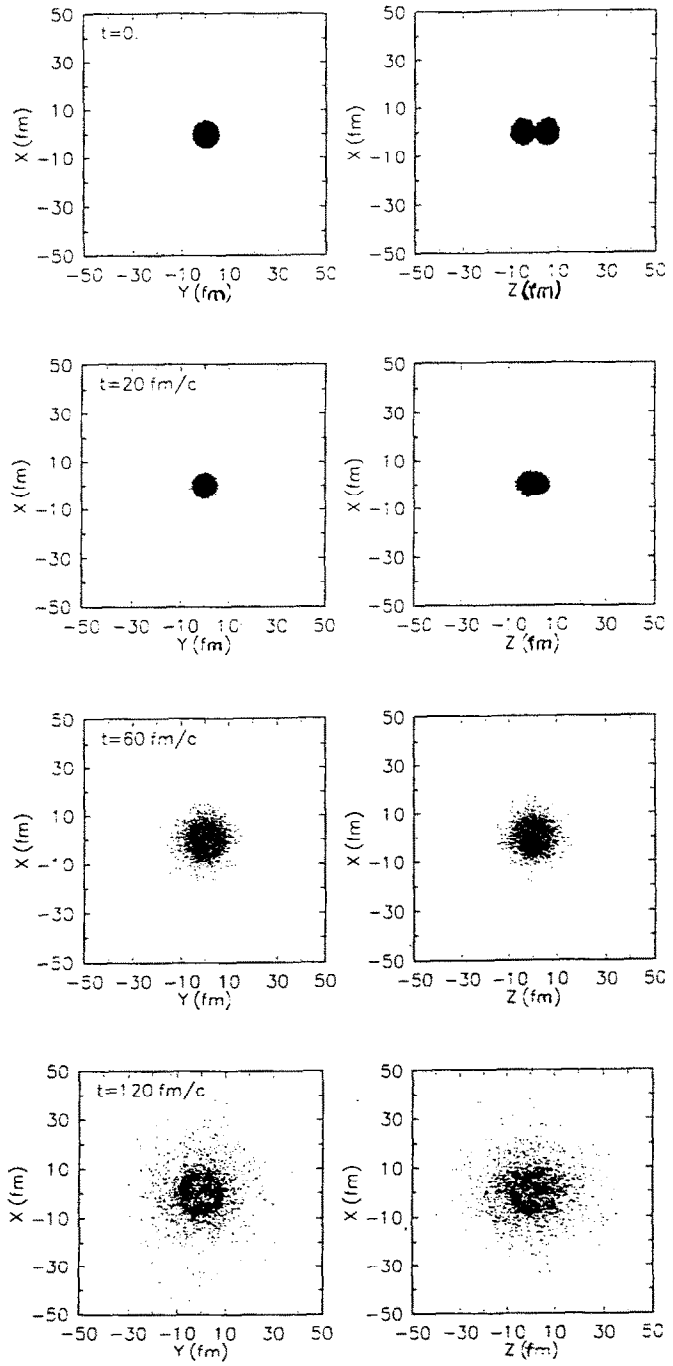


Fig. 2. Scatter plots of the one-body density distribution for $^{96}$Mo+$^{96}$Mo reactions at a beam energy of 55 MeV/nucleon. The calculation is done with $K = 200$ MeV and with the Coulomb interaction.

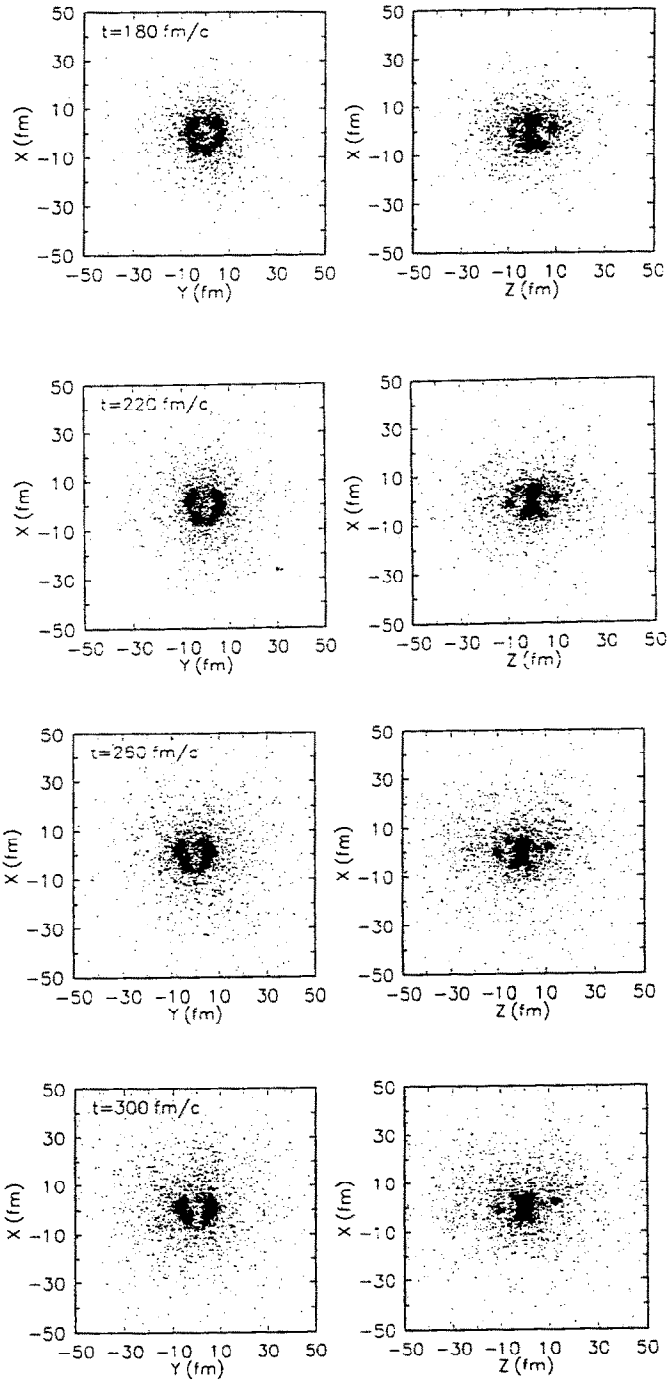


Fig. 2—continued

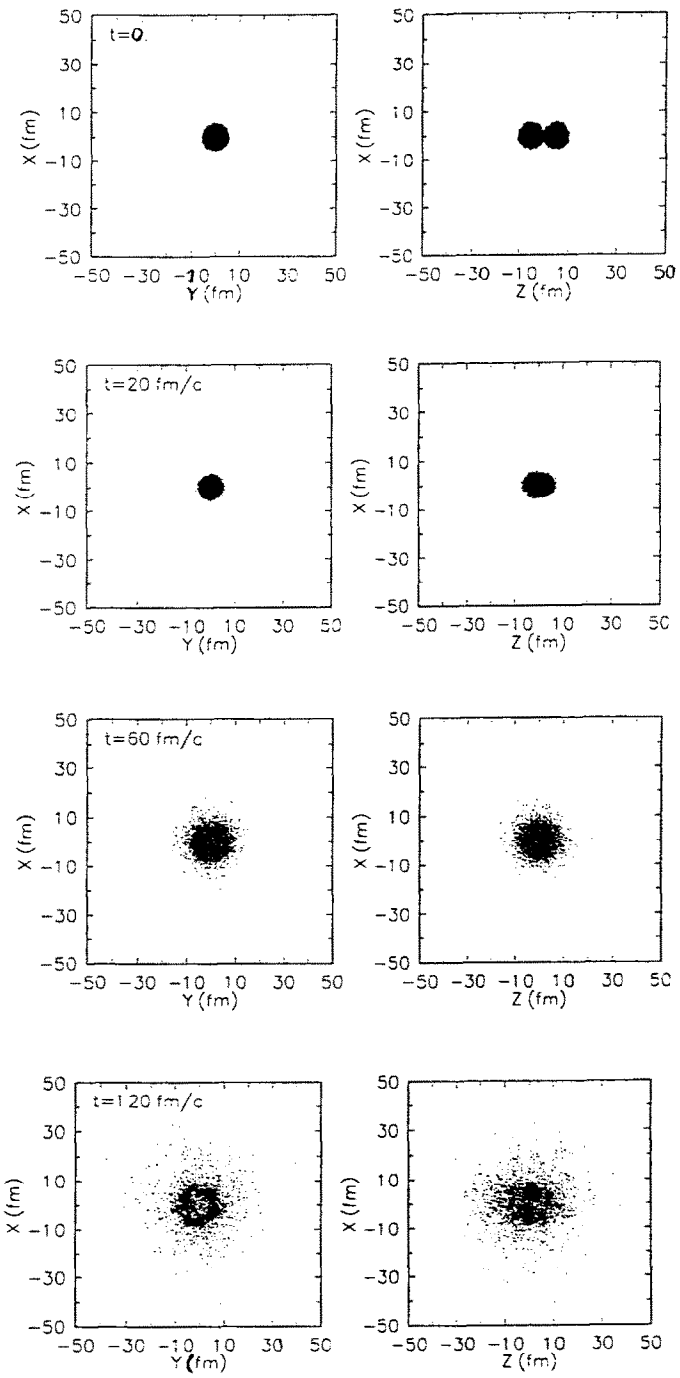


Fig. 3. Scatter plots of the one-body density distribution for $^{96}$Mo+$^{96}$Mo reactions at a beam energy of 55 MeV/nucleon. The calculation is done with $K = 200$ MeV and without the Coulomb interaction.

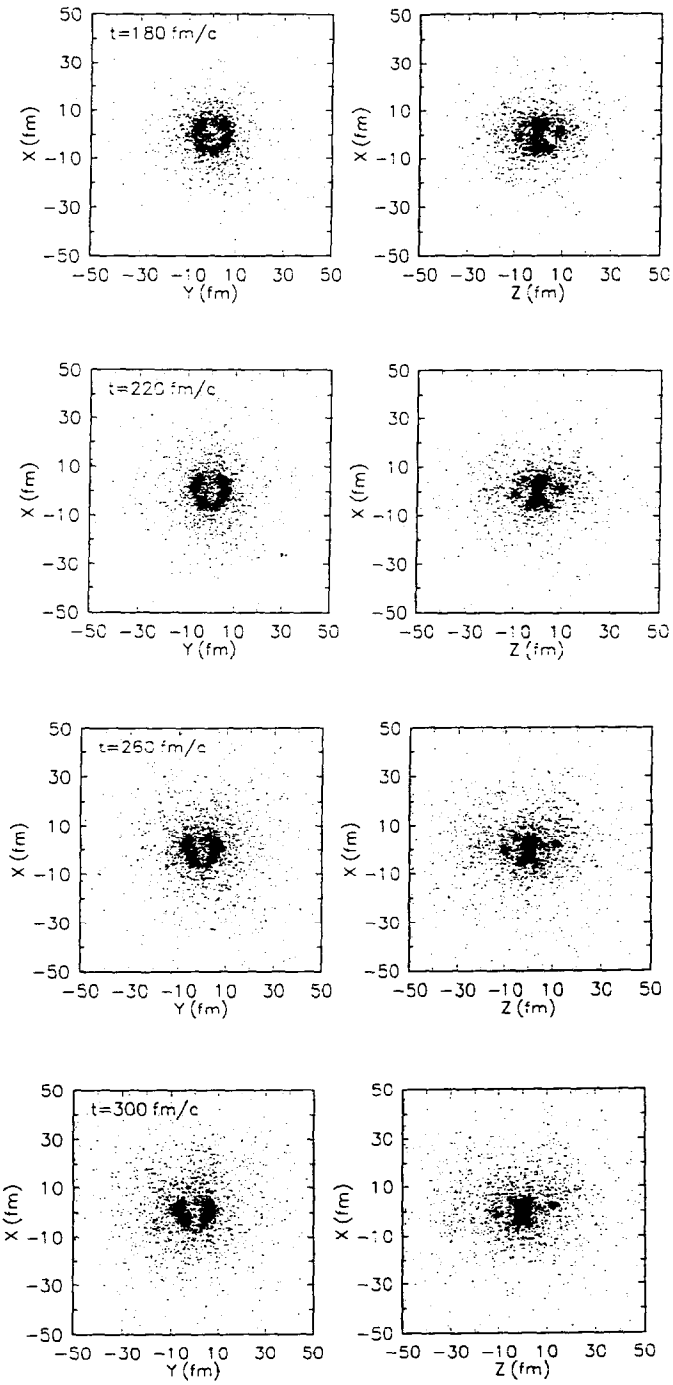


Fig. 3—continued

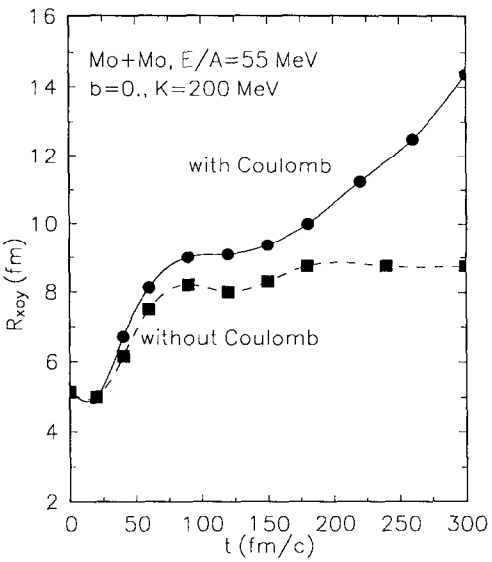


Fig. 4. The radii of the dense part of the one-body density profiles shown in figs. 2 and 3.

these fragments from the center of mass. We clearly see the expansion from the initial compression up to the radius of about normal nuclear matter density at about 60 fm/$c$ where a substantial part of the nucleons start to leave the dense region as fast preequilibrium nucleons. *From here on the remaining ensemble of dense fragments creeps extremely slowly outwards up to it reaches a radius of* $R \approx 2A^{1/3}$ *at* $\approx 150$ *fm/c from where on the system explodes in the calculation with Coulomb repulsion.* It is very suggestive to interpret this "creeping phase as a chaotic expansion of a fragmenting nucleus with a strong dissipation of energy into the new surfaces which finally terminates at $R \approx 2A^{1/3}$, the freeze-out point. This comes close to the picture described in refs. [55,56,2]).

(3) In contrast to the dynamics with Coulomb there is no further expansion without Coulomb repulsion beyond the freeze-out radius. On the contrary, the ensemble of dense fragments dissolves slowly due to further nucleon evaporation and even shrinks. The initial compression seems not to lead to a blowing up of the dense part of the system. All collective flow within this part seems to be completely dissipated during the strongly dissipative period of fragmentation.

As we have seen here the occurrence of the fragmentation phenomenon strongly depends on the initial compression and subsequent expansion, these, however, are intimately determined by the compressibility coefficient and the beam energy used in the model calculations. It is therefore interesting to study how the fragmentation pattern depends on the compressibility coefficient $K$ and the beam energy. The geometry of the final-fragment distribution might be studied experimentally through

the fragment-fragment correlation function which in turn might provide an experimental constraint on the nuclear equation of state [65]).

First, we show in figs. 5 and 6 scatter plots of the one-body density distributions obtained by using $K = 380$ and 540 MeV, respectively. The beam energy is again 55 MeV/nucleon and all the calculations are done with the Coulomb interaction. It is seen that the density distributions in the reaction plane ($xz$ plane) are oblate due to the squeezing-out of nuclear matter in the initial compression phase. As we can see from fig. 1 nuclear matter is hard to compress with higher compressibility coefficients. In the planes ($xy$ planes) perpendicular to the beam direction there are holes developing, the overall shape of the density distribution resembles that of a doughnut. Similar behaviour has also been observed in Moretto's calculations with high compressibility coefficients. To see quantitatively effects of the nuclear equation of state on the radius of the dense part of the density distribution, we present in fig. 7 the radius as a function of time for the three compressibility coefficients $K$. In the initial compression and early expansion phases the three equations of states give rather similar results, after about 50 fm/$c$ the difference begins to show up. For the $K = 380$ and 540 MeV cases the radius stays about constant for a short time, then it decreases due to continuous particle emission and the shrinking of holes in the middle. Apparently, with the high compressibility coefficients and a beam energy of 55 MeV/nucleon the initial compression is small and therefore the radial kinetic energy in the expansion phase is also smaller than the binding energy of nucleons, no Coulomb explosion is observed.

To show the energy dependence of the fragmentation pattern in our model calculations, we show in figs. 8–10 the scatter plots for the $^{96}$Mo+$^{96}$Mo reactions at a beam energy of 100 MeV/nucleon with $K = 200$, 380 and 540 MeV, respectively. The radii extracted from the scatter plots are shown in fig. 11. Here we see that the whole system disintegrated into small fragments and single nucleons, this is because the radial expansion energy obtained at this energy after the initial compression is much larger than the binding energy of nucleons. The expanding velocity of the dense part of the system shows a slight slow down at about 100 fm/$c$ as one can see from the slope of the radii as a function of time. With the high compressibility $K$'s the final fragments distribute in a more deformed oblate volume compared to that in the $E/A = 55$ MeV case.

Wong proposed the formation of bubble nuclei at high excitations due to the Coulomb repulsion [36]). It may be that the bubbles seen in our calculations at a beam energy of 55 MeV/nucleon with high compressibility coefficients are linked to the same phenomenon. However, they appear at later times much after the instabilities showed up. It is highly doubtful whether a reduced single-particle dynamics like BUU is able to describe the time evolution of the system correctly in spite of the considerable large many-body correlations that have been built up by the fragmentation.

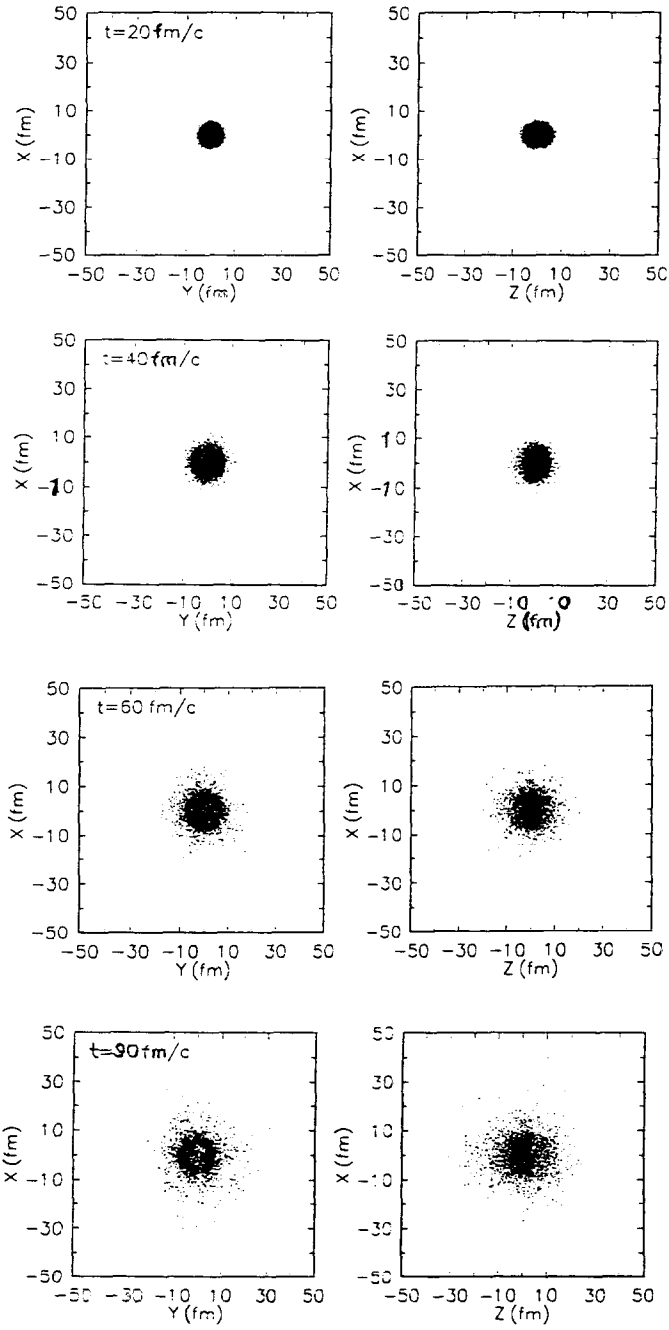


Fig. 5. Scatter plots of the one-body density distribution for $^{96}$Mo + $^{96}$Mo reactions at a beam energy of 55 MeV/nucleon. The calculation is done with $K = 380$ MeV and with the Coulomb interaction.

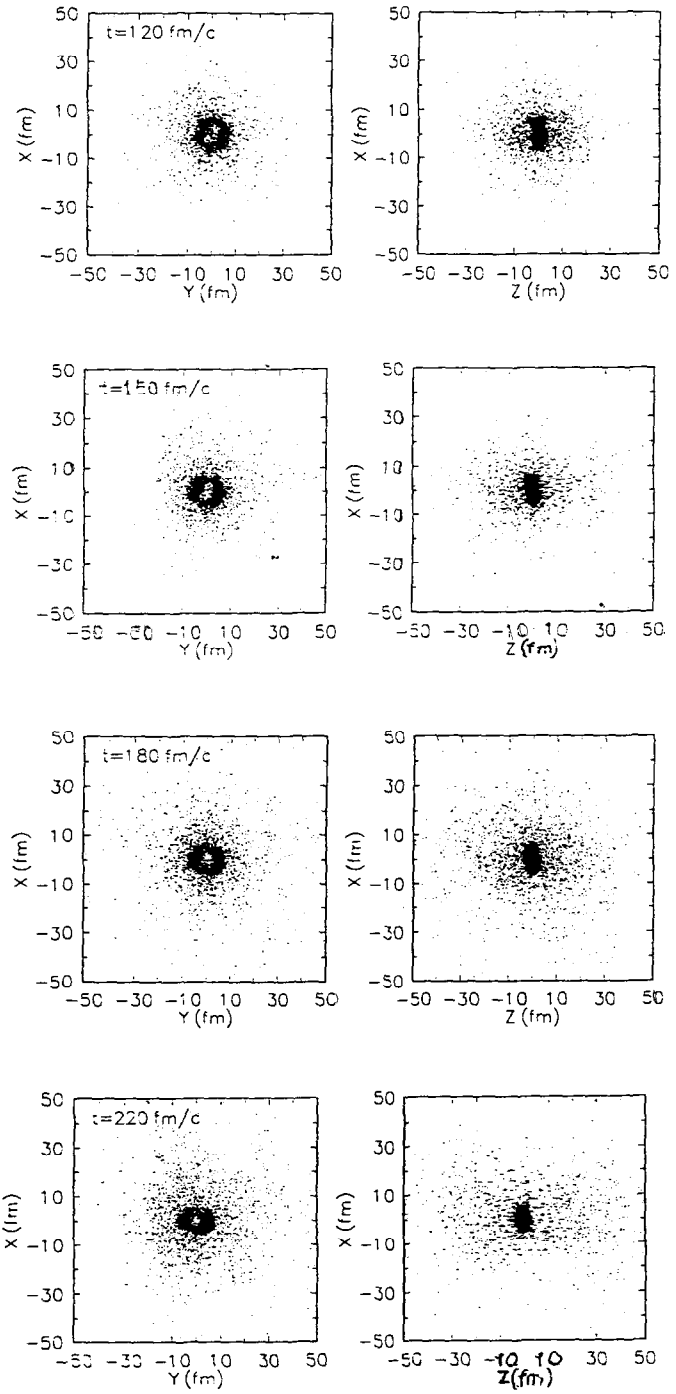


Fig. 5—continued

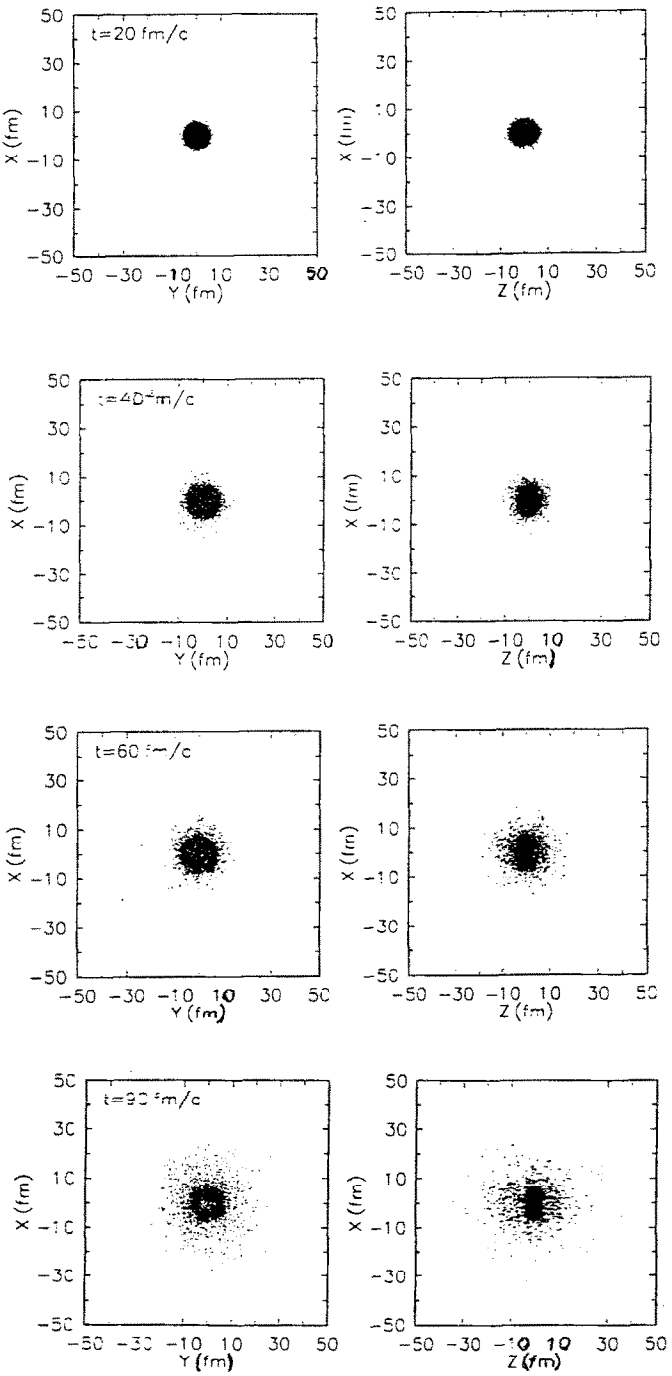


Fig. 6. Scatter plots of the one-body density distribution for $^{96}$Mo+$^{96}$Mo reactions at a beam energy of 55 MeV/nucleon. The calculation is done with $K = 540$ MeV and with the Coulomb interaction.

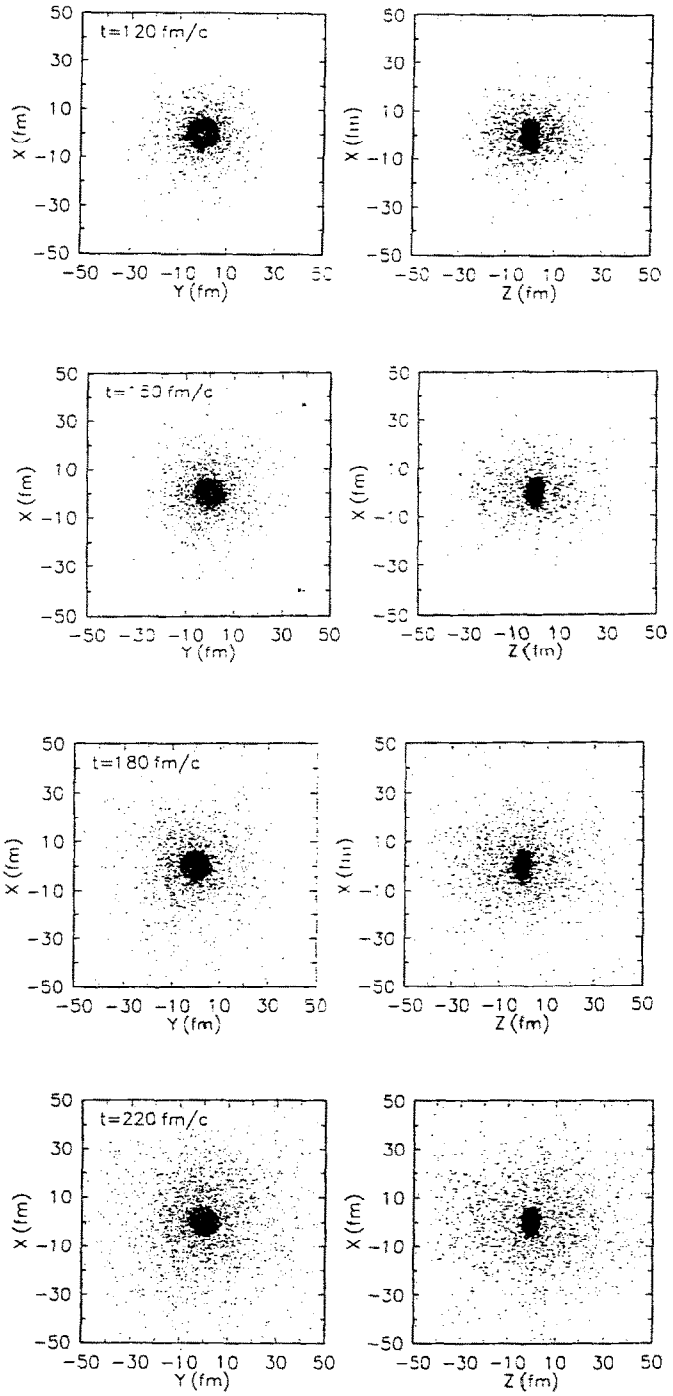


Fig. 6—continued

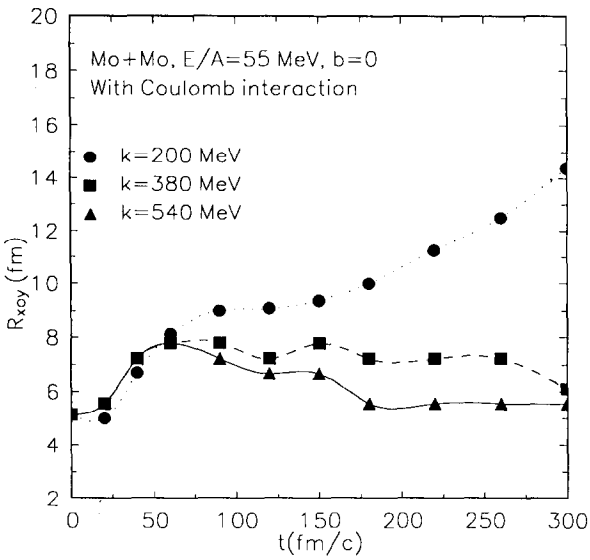


Fig. 7. The comparison of the radii of the dense part of the one-body distributions calculated at $E/A = 55$ MeV/nucleon with the three different compressibility coefficients.

### 3.2. THE ADIABATIC SOUND VELOCITY

The fragmentation we see here is triggered by fluctuations generated during the reaction process via nucleon-nucleon collisions and that from the initial distribution of test particles in phase space via a Monte Carlo sampling. They are further propagated through the mean field and subsequent nucleon-nucleon collisions. Whether these fluctuations can result in the disintegration of the reaction system depends on whether the density and temperature reached in the expansion phase can reach the hydrodynamical instability region or not. We study this problem by following the adiabatic sound velocity in the reaction process within a sphere surrounding the center of mass with a radius of 2.0 fm.

Our results on the adiabatic sound velocity are shown in figs. 12 and 13 for the beam energy of 55 and 100 MeV/nucleon, respectively. It is seen that the sound velocity becomes imaginary at about 50 and 35 fm/$c$, respectively. The zero value of the adiabatic sound velocity in the later stage of the reaction is due to the zero density in the case of bubble formation and it may become real again due to the closing up of the bubble. The time when the sound velocity becomes imaginary is, however, not so sensitive to the compressibility coefficient used. It is interesting to note that the dynamical instabilities characterized by the imaginary adiabatic sound velocity already occurred when the density profile looks rather normal before the

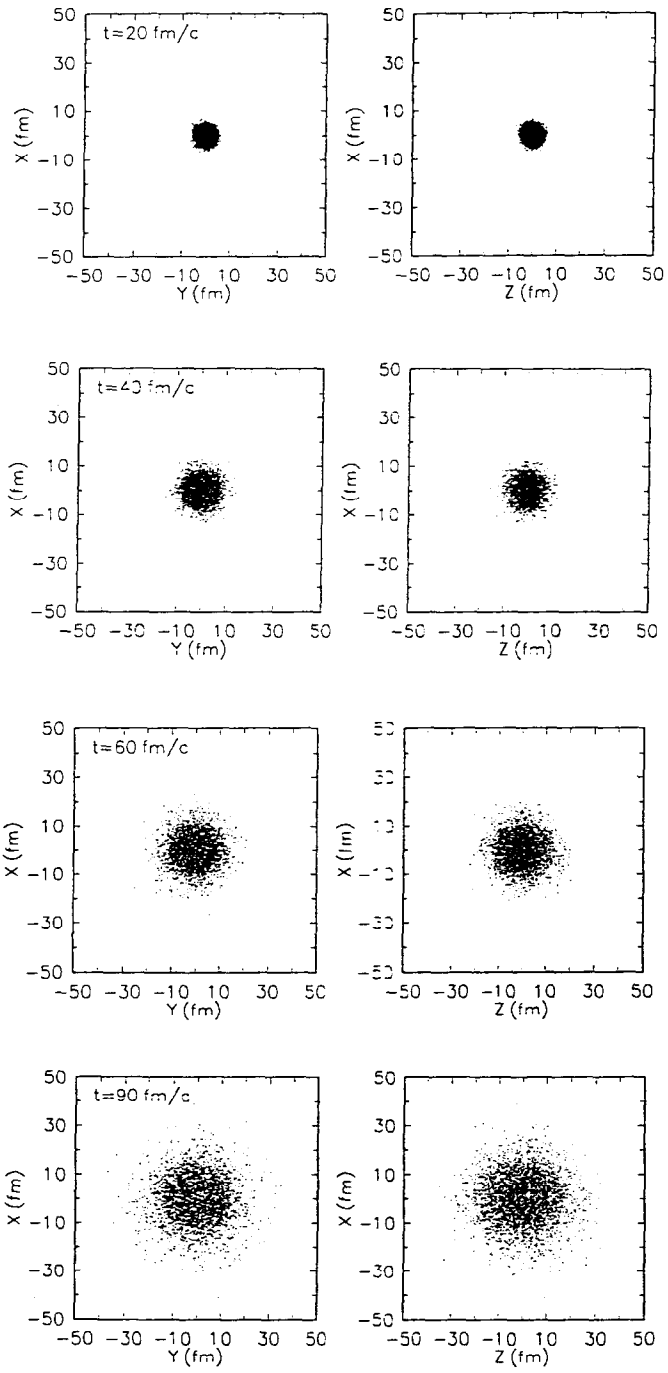


Fig. 8. Scatter plots of the one-body density distribution for $^{96}$Mo+$^{96}$Mo reactions at a beam energy of 100 MeV/nucleon. The calculation is done with $K = 200$ MeV and with the Coulomb interaction.

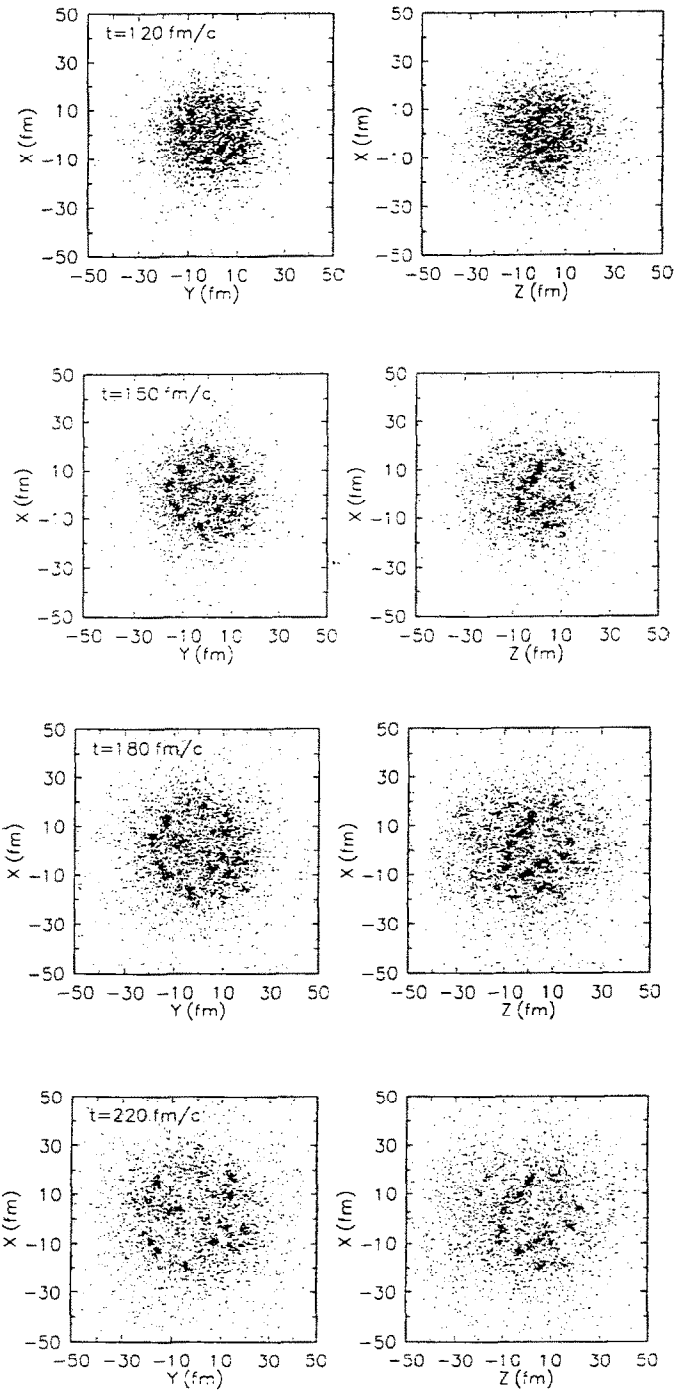


Fig. 8—continued

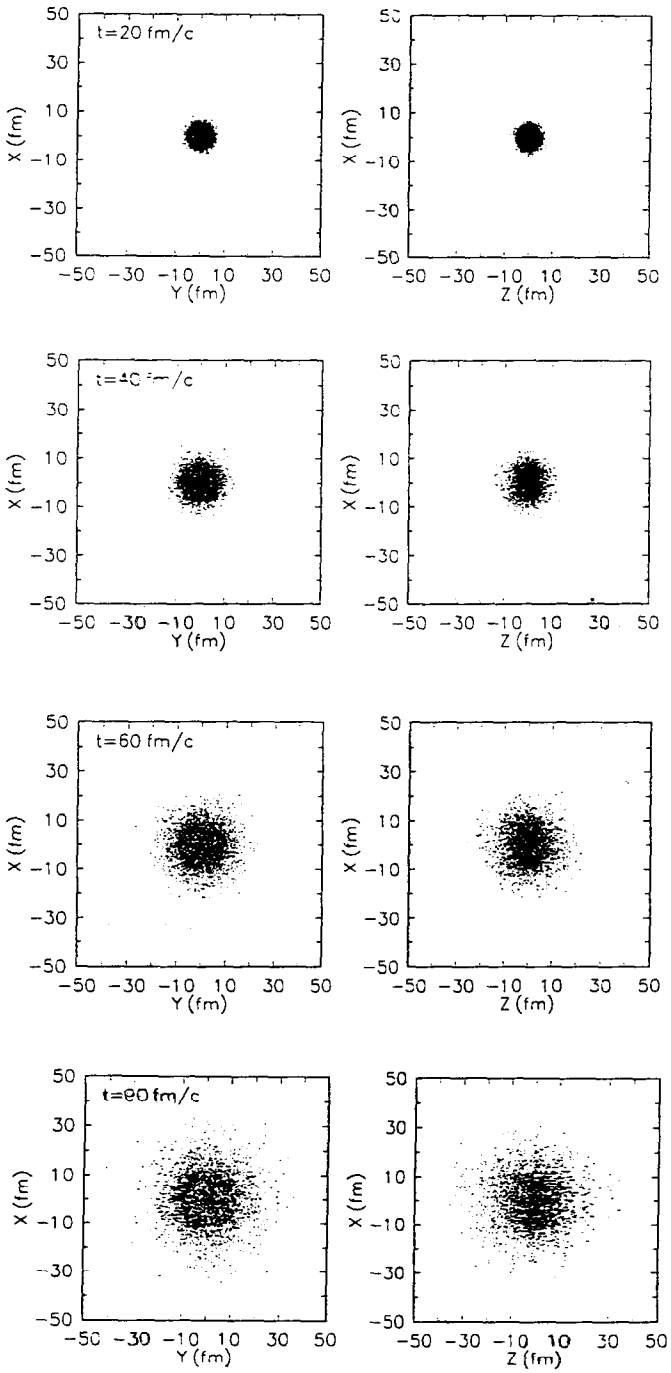


Fig. 9. Scatter plots of the one-body density distribution for $^{96}$Mo + $^{96}$Mo reactions at a beam energy of 100 MeV/nucleon. The calculation is done with $K = 380$ MeV and with the Coulomb interaction.

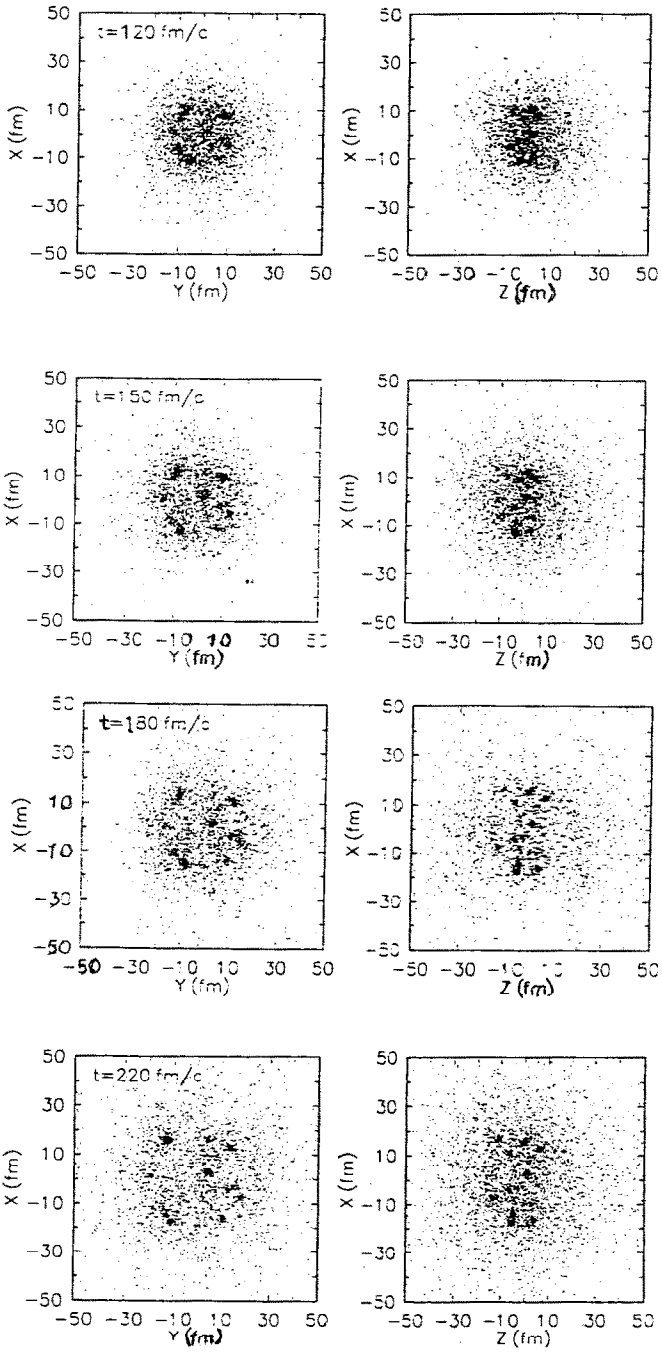


Fig. 9—continued

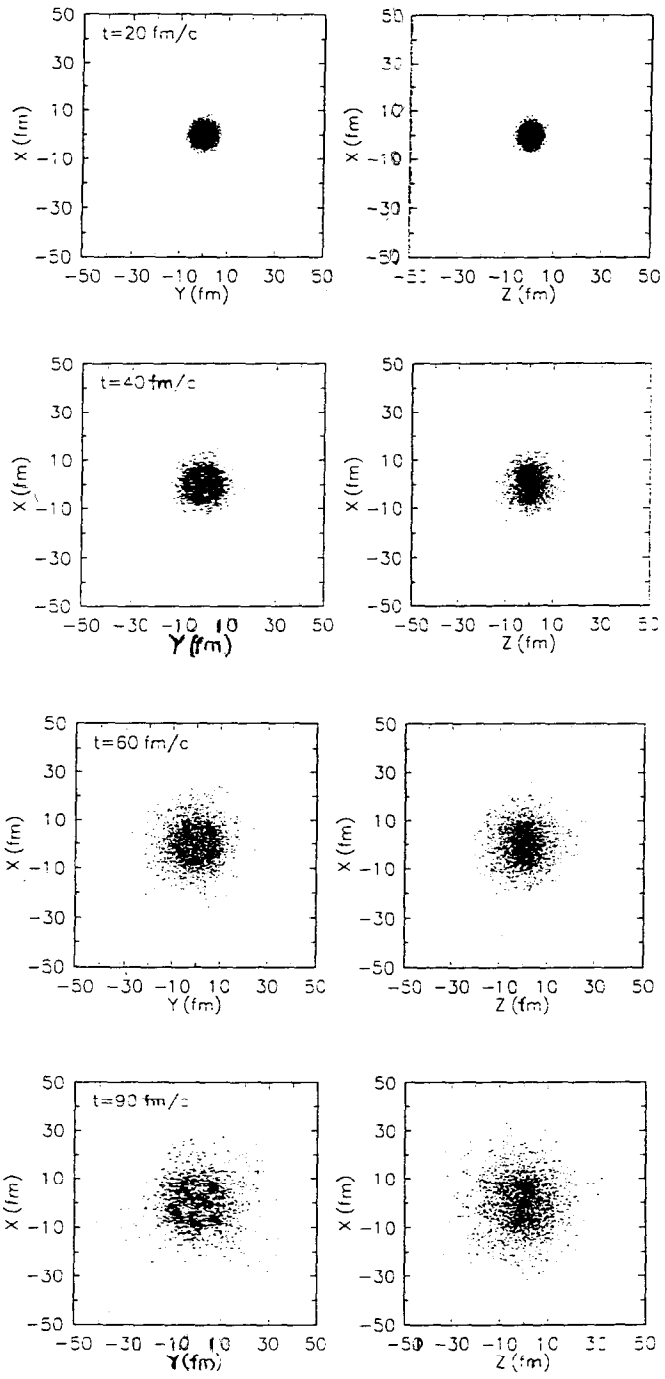


Fig. 10. Scatter plots of the one-body density distribution for $^{96}$Mo+$^{96}$Mo reactions at a beam energy of 100 MeV/nucleon. The calculation is done with $K = 540$ MeV and with the Coulomb interaction.

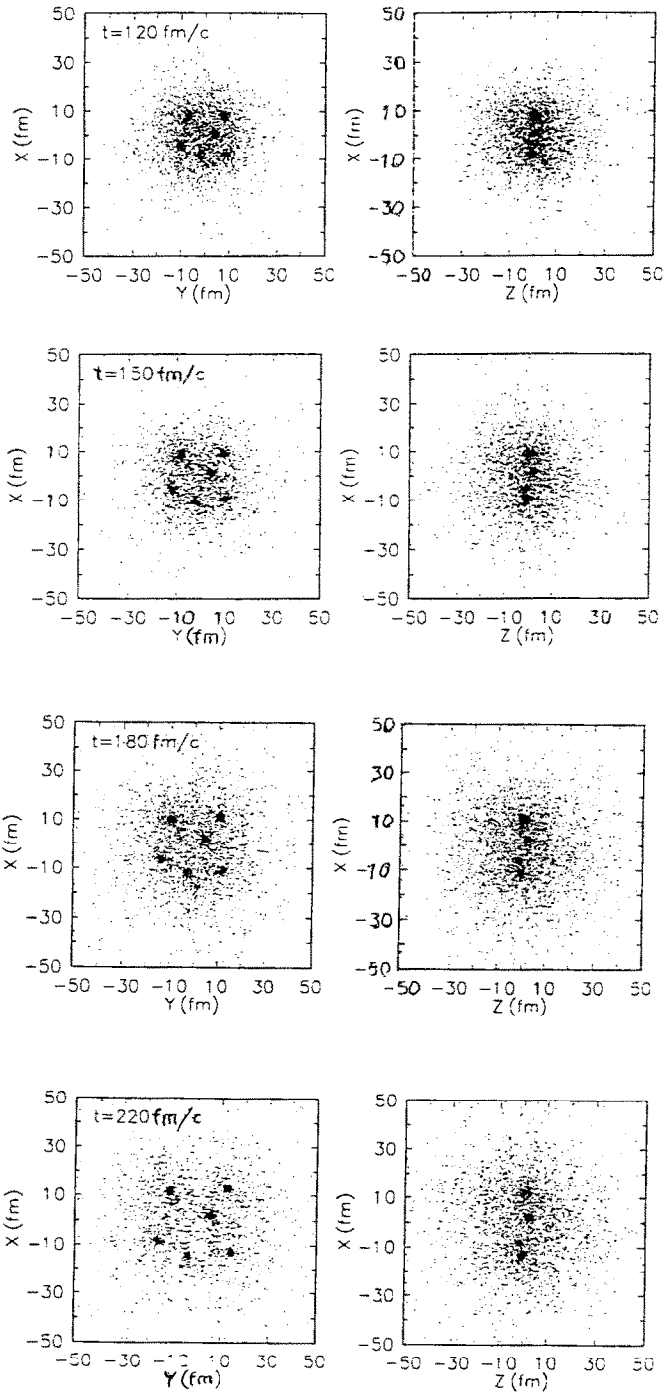


Fig. 10—continued

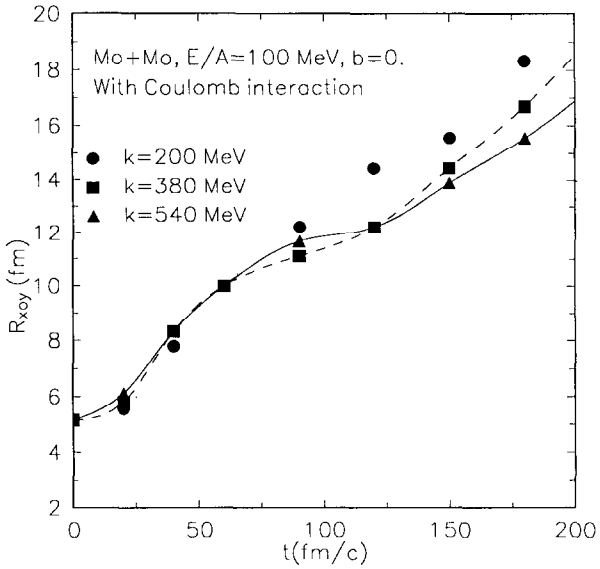


Fig. 11. The radii of the dense part of the one-body as shown in figs. 8-10.

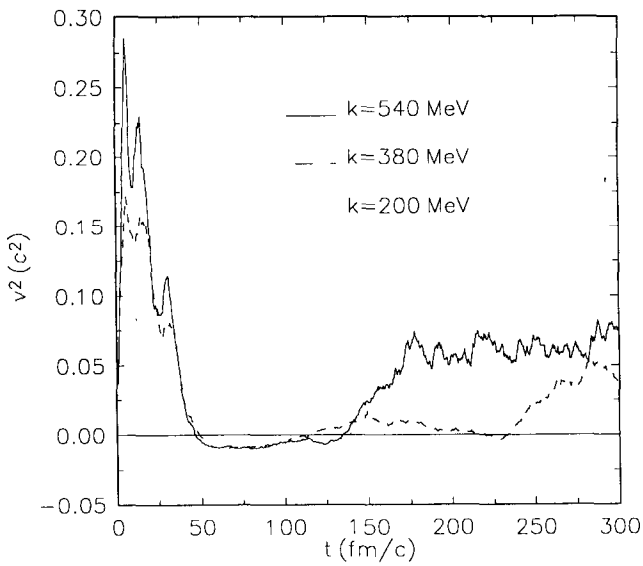


Fig. 12. The square of the adiabatic sound velocity calculated for $E/A = 55$ MeV with the three different compressibility coefficients.

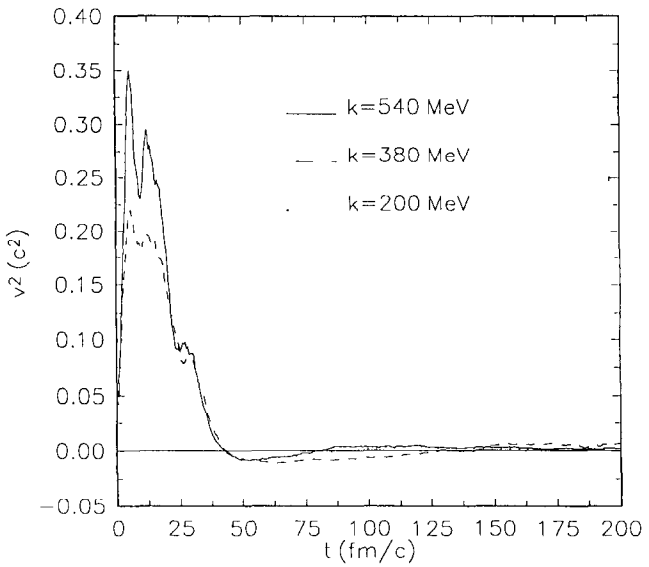


Fig. 13. The square of the adiabatic sound velocity calculated for $E/A = 100$ MeV with the three different compressibility coefficients.

bubbles or fragments appear. This finding is in agreement with that found by Ngô *et al.* [37]). That means *the instabilities against fragmentation are coming very early in the BUU dynamics.*

### 3.3. THERMALIZATION OF HEAVY RESIDUES

To practically study properties of final fragments and compare with experimental data we propose a hybrid model by coupling the BUU model with a statistical model. The necessary condition for a statistical model to be applicable is the establishment of a more or less thermalized source. For this purpose we study the relaxation of the quadrupole moment in momentum space for particles in a sphere of radius $R$ shown in fig. 7 and fig. 11. In terms of the nucleonic phase-space distribution function $f(\boldsymbol{r}, \boldsymbol{p}, t)$, the quadrupole moment is defined as

$$Q_{zz}(t) = \int \frac{\mathrm{d}\boldsymbol{r}\,\mathrm{d}\boldsymbol{p}}{(2\pi)^3}(2p_z^2 - p_x^2 - p_y^2) f(\boldsymbol{r}, \boldsymbol{p}, t)\,. \tag{9}$$

Thermalization of nuclear systems at beam energies around 1.0 GeV/nucleon was studied in cascade models [30,32]) and the BUU model [57]) by studying the relaxation of the quadrupole moment. At beam energies around 100 MeV/nucleon, it was also studied in the BUU model [49,58]) and more recently in the QMD model [59]). In figs. 14 and 15 we show the quadrupole moment together with the number of

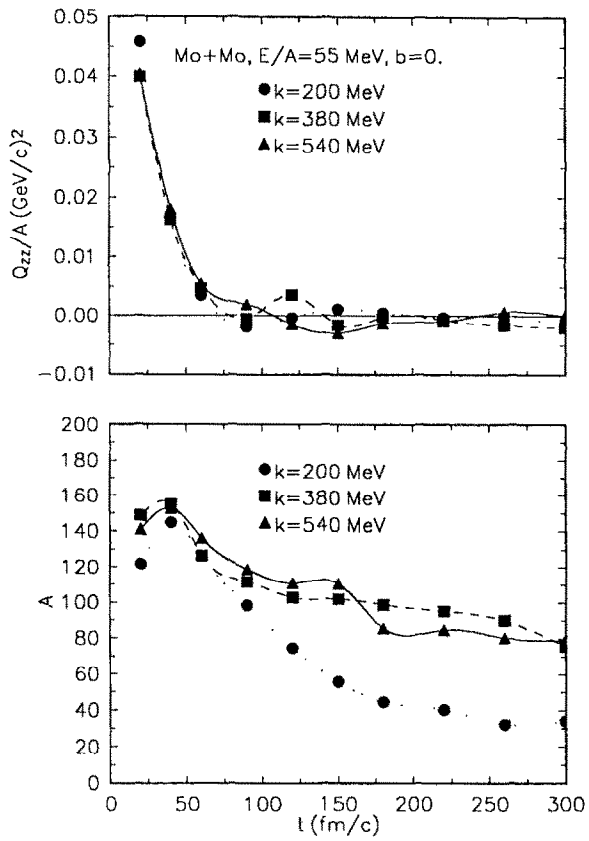


Fig. 14. The quadrupole moment and the mass number of nucleons in a sphere of radius $R$ surrounding the center of mass. The calculation is done for $E/A = 55$ MeV with the three different compressibility coefficients.

nucleons in the sphere of radius $R$ as a function of time for the reaction of $^{96}$Mo+$^{96}$Mo at a beam energy of 55 and 100 meV/nucleon, respectively. It is seen that the quadrupole moment becomes about zero at about 100 and 60 fm/$c$ for $E/A = 55$ and 100 MeV/nucleon, respectively, for all of the three compressibility coefficients. It indicates that a thermal equilibrium is reached in the sphere at both of the beam energies. Our findings here on the thermalization of heavy residue in intermediate-energy heavy-ion collisions are in agreement with that of Aichelin and Stöcker [64]) as well as Bauer [49]). It is interesting to note that, in recent experimental studies [60-62]) by measuring the excited-state population of intermediate-mass fragments in conjunction with a charged-particle multiplicity filter, it was found that rather complete thermalization has been established in central heavy-ion collisions at beam energies around 50 MeV/nucleon. The same conclusion was drawn from the result of the recent experiment on the fragmentation of projectile spectators in

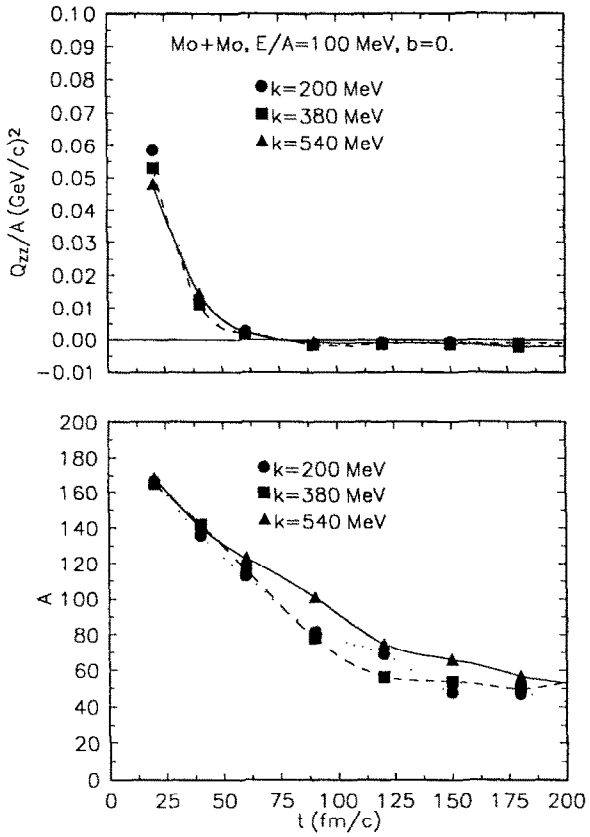


Fig. 15. The quadrupole moment and the mass number for nucleons in a sphere of radius $R$ surrounding the center of mass. The calculation is done for $E/A = 100$ MeV with the three different compressibility coefficients.

600$A$ MeV $^{197}$Au on various light targets [11,63]) by measuring the ratio of velocities in the longitudinal and transverse directions.

## 4. Summary

In summary, we have studied systematically the onset of dynamical instabilities and nuclear multifragmentation in central collisions of $^{96}$Mo + $^{96}$Mo at beam energies of 55 and 100 MeV/nucleon by simulating numerically the reaction dynamics of intermediate-energy heavy-ion collisions within the Boltzmann-Uehling-Uhlenbeck (BUU) transport model. We found dynamical instabilities characterized by an imaginary adiabatic sound velocity in the central region of the reaction developed very early during the expansion phase of the reaction. We have also studied the thermalization of the dense part of the one-body density profile, it is found that

*also a rather complete thermalization is established when the dynamical instabilities set in* for the central collisions of $^{96}$Mo+$^{96}$Mo. As BUU is non-linear, significant fluctuations and correlations can grow and signal a transition to a new dynamics.

Here a highly equilibrized, non-adiabatic expansion and fragmentation starts. Freeze-out, as assumed in the statistical model [2]) will be at the end of this. Fragmentation is accompanied by a build up of many-body correlations ignored in the BUU model. Thus these instabilities also signal the break-down of the validity of BUU. Only, if the many-body correlations do not significantly modify the time evolution of the single-particle distribution, one can follow the BUU dynamics further.

We studied systematically multifragmentation patterns at two beam energies and three different compressibility coefficients by making scatter plots of the one-body density distributions. Up to about 100 MeV/$c$ the evolution of the system is rather similar. In every case fragmentation and the occurrence of an imaginary sound velocity happens much earlier.

Later on, following BUU further with all reservations mentioned above, the fragmentation patterns and the geometry of the final-fragment distribution become different at different beam energies and compressibility coefficients. At a beam energy of 55 MeV/nucleon by using of a soft nuclear equation of state of the compressibility coefficient $K = 200$ MeV, a scatter plot of the one-body density distribution shows after the breaking into "fragments", a very slow creeping expansion up to a freeze-out and in the case of included Coulomb interaction a Coulomb explosion. At the same beam energy but $K = 380$ and 540 MeV, we observed the creation and disappearance of bubbles, no Coulomb explosion is observed. At a beam energy of 100 MeV/nucleon, with all the three compressibility coefficients of $K = 200$, 380 and 540 MeV, the initial compression is so high that the whole system blows up into small fragments and single nucleons. The final fragments and nucleons populate a volume with oblate deformation. The deformation of the volume is larger with higher beam energies or higher compressibility coefficients.

We would like to thank W. Bauer, A.R. DeAngelis, U. Mosel, J. Nemeth, J. Randrup and C.Y. Wong for helpful discussions. We are grateful to the Deutsche Forschungemeinschaft for continuous generous financial support.

## References

1) D.H.E. Gross, invited talk for the International Nuclear Physics Conference, 26 July-1 August 1992, Wiesbaden, Germany, to appear in Nucl. Phys. **A**
2) D.H.E. Gross, Rep. Progr. Phys. **53** (1990) 605, and references therein
3) P.J. Siemens, Nature **305** (1983) 410
4) J.A. Lopez and P.J. Siemens, Nucl. Phys. **A431** (1984) 728
5) L. Goodman, J.I. Kapusta and A.Z. Mekjian, Phys. Rev. **C30** (1984) 851
6) B.A. Li, S. Pratt and P.J. Siemens, Phys. Rev. **C37** (1988) 728
7) G. Bertsch and P.J. Siemens, Phys. Lett. **B126** (1983) 9

8) C.J. Pethick and D.G. Ravenhall, Nucl. Phys. **A471** (1987) 19c;
H. Heiselberg, C.J. Pethick and D.G. Ravenhall, Nucl. Phys. **A519** (1990) 279c, and references therein
9) S. Fin *et al.*, Phys. Lett. **B49** (1982) 1321
10) D.R. Bowman, G.F. Peaslee, R.T. de Souza, N. Carlin, G.K. Gelbke, W.G. Gong, C.D. Kim, M.A. Lisa, W.G. Lynch, L. Phair, M.B. Tsang, C. Williams, N. Colonna, K. Hanold, M.A. McMahan, G.J. Wozniak, L.G. Moretto and W.A. Friedman, Phys. Rev. Lett. **67** (1991) 1527
11) C.A. Ogilvie, J.C. Adloff, M. Begemann-Blaich, P. Boissou, J. Hubele, G. Imme, I. Iori, P. Kreutz, G.J. Kunde, S. Leray, V. Lindenstruth, Z. Liu, U. Lynen, R.J. Meijer, U. Milkau, W.F. Müller, C. Ngô, J. Pochodzalla, G. Raciti, G. Rudolf, H. Sann, A. Schüttauf, W. Seidel, L. Stuttge, W. Trautmann and A. Tucholski, Phys. Rev. Lett. **67** (1991) 1214
12) K. Hagel, M. Gonin, R. Wada, J.B. Natowitz, Y. Lou, J. Ruiz, D. Drain, B. Chambon, B. Cheynis, D. Guinet, X.C. Hu, A. Demeyer, C. Pasteur, A. Giorni, A. Lieres, P. Stassi, B. Viano and P. Gonthier, Progress in Research, Cyclotron Institute Texas A&M University, College Station, Texas (1991) p. 18
13) J.P. Alard *et al.* Phys. Rev. Lett. **69** (1992) 889
14) J. Randrup and S.E. Koonin, Nucl. Phys. **A356** (1981) 223
15) D.H.E. Gross *et al.*, Z Phys. **A309** (1982) 41;
D.H.E. Gross and X.Z. Zhang, Phys. Lett. **B161** (1985) 47;
X.Z. Zhang, D.H.E. Gross, S.Y. Xu and Y.M. Zheng, Nucl. Phys. **A461** (1987) 668
16) J.P. Bondorf, Nucl. Phys. **A387** (1982) 25c
17) G. Fai and J. Randrup, Nucl. Phys. **A381** (1982) 557; Phys. Lett. **B115** (1982) 281; Nucl. Phys. **A404** (1983) 281
18) J. Hüfner, Phys. Reports **125** (1985) 131
19) W. Bauer *et al.*, Phys. Lett. **B150** (1985) 53; Nucl. Phys. **A452** (1986) 699;
W. Bauer, Phys. Rev. **C38** (1988) 1927
20) L. Phair, W. Bauer, D.R. Bowman, N. Carlin, R.T. de Souza, C.K. Gelbke, W.G. Gong, Y.D. Kim, M.A. Lisa, W.G. Lynch, G.F. Peaslee, M.B. Tsang, C. Williams, F. Zhu, N. Colonna, K. Hanold, M.A. McMahan, G.J. Wozniak and L.G. Moretto, Phys. Lett. **B285** (1992) 10
21) W. Bauer, D.R. Bowman, N. Carlin, R.T. de Souza, C.K. Gelbke, W.G. Gong, Y.D. Kim, M.A. Lisa, W.G. Lynch, M.A. McMahan, L.G. Moretto, G.F. Peaslee, L. Phair, M.B. Tsang, C. Williams, G.J. Wozniak and F. Zhu, Book of Abstracts of the International Nuclear Physics Conference, Wiesbaden, Germany, 26 July–1 August 1992, p. 3.4.20
22) A. Vincentini, G. Jaccucci and V.R. Pandharipande, Phys. Rev. **C31** (1985) 1783
23) J. Aichelin, Phys. Reports **202** (1991) 233
24) G. Bertsch and S. Das Gupta, Phys. Reports **160** (1988) 233
25) H. Stöcker and W. Greiner, Phys. Reports **137** (1986) 277
26) W. Bauer, G.F. Bertsch and S. Das Gupta, Phys. Rev. Lett. **58** (1987) 863
27) S. Ayik and C. Gregoire, Phys. Lett. **B212** (1988) 269; Nucl. Phys. **A513** (1990) 187
28) Ph. Chomaz, G.F. Burgio and J. Randrup, Phys. Lett. **B254** (1991) 340;
G.F. Burgio, Ph. Chomaz and J. Randrup, Nucl. Phys. **A529** (1991) 157
29) C. Gale and S. Das Gupta, Phys. Lett. **B162** (1985) 35;
S. Das Gupta, C. Gale and J. Gallego, Phys. Rev. **C33** (1986) 1634
30) J. Randrup, Nucl. Phys. **A314** (1979) 429
31) Y. Yariv and Z. Fraenkel, Phys. Rev. **C20** (1979) 2227
32) J. Cugnon, Phys. Rev. **C22** (1980) 1885;
J. Cugnon, T. Mizutani and J. Vandermeulen, Nucl. Phys. **A352** (1981) 505;
J. Cugnon, D. Kinet and J. Vandermeulen, Nucl. Phys. **A379** (1982) 553;
M. Cahay, J. Cugnon and J. Vandermeulen, Nucl. Phys. **A411** (1983) 524;
J. Cugnon and M.C. Lemaire, Nucl. Phys. **A489** (1988) 781
33) C.Y. Wong, Phys. Rev. **C25** (1982) 1460
34) L. Vinet, C. Gregoire and P. Schuck, Nucl. Phys. **A468** (1987) 321
35) C. Gregoire, B. Remaud, F. Sebille, L. Vinet and Y. Raffray, Nucl. Phys. **A465** (1987) 317; Phys. Lett. **B180** (1986) 198
36) C.Y. Wong, Phys. Rev. Lett. **55** (1985) 1973

37) C. Ngô, H. Ngô, S. Leray and M.E. Spina, Nucl. Phys. **A499** (1989) 148
38) J. Nemeth, M. Barranco, C. Ngô and E. Tomasi; Z. Phys. **A323** (1986) 419
39) D. Boal and J. Glosli, Phys. Rev. **C42** (1990) R502
40) B. Strack and J. Knoll, Z. Phys. **315** (1984) 249;
J. Knoll and B. Strack, Phys. Lett. **B149** (1984) 45;
J. Knoll and J.S. Wu, Nucl. Phys. **A481** (1988) 173
41) G.F. Burgio, Ph. Chomaz and J. Randrup, Phys. Rev. Lett. **69** (1992) 885
42) L.G. Moretto, K. Tsuo, N. Colonna and G.J. Wozniak, Phys. Rev. Lett. **69** (1992) 1884
43) W. Bauer, G.F. Bertsch and H. Schultz, Phys. Rev. Lett. **69** (1992) 1888
44) D.H.E. Gross, B.A. Li, and A.R. DeAngelis, Ann. der Phys. **1** (1992) 467
45) A. Bonasera, G.F. Burgio and M. DiToro, Phys. Lett. **B221** (1989) 233;
A. Bonasera, G. Russo and H.H. Wolter, Phys. Lett. **B246** (1990) 337
46) S.J. Wang and W. Cassing, Ann. of Phys. **159** (1985) 328
47) S.J. Wang, B.A. Li, W. Bauer and R. Randrup, Ann. of Phys. **209** (1991) 251
48) W. Bauer *et al.*, Phys. Rev. **C34** (1986) 2127;
W. Bauer, C.K. Gelbke and S. Pratt, Annu. Rev. Nucl. Part. Sci. **42** (1992) 77
49) W. Bauer, Phys. Rev. Lett. **61** (1988) 2534
50) B.A. Li and W. Bauer, Phys. Lett. **B254** (1991) 335; Phys. Rev. **C44** (1991) 450;
B.A. Li, W. Bauer and G.F. Bertsch, Phys. Rev. **C44** (1991) 2095;
W. Bauer and B.A. Li, *in* Proc. Workshop on Relativistic Aspects of Nuclear Physics, Rio de Janeiro; 28–30 August 1991, ed. T. Kodama *et al.* (World Scientific, Singapore) p. 229
51) J.P. Blaizot, Phys. Reports **64** (1980) 171
52) M.M. Sharma, W.T.A. Borghols, S. Brandenburg, S. Crona, A. van der Woude and M.N. Harakeh, Phys. Rev. **C38** (1988) 2562
53) C. Gale, G.F. Bertsch and S. Das Gupta, Phys. Rev. **C35** (1987) 1666
54) P.J. Siemens and J. Kapusta, Phys. Rev. Lett. **43** (1979) 1486;
J. Kapusta, Phys. Rev. **C29** (1984) 1735;
H. Schulz, G. Röpke, K.K. Gudima and V.D. Toneev, Phys. Rev. **C34** (1986) 1294;
L.P. Csernai, J.I. Kapusta, G. Fai, D. Hahn, J. Randrup and H. Stöcker, Phys. Rev. **C35** (1987) 1297;
P. Danielewicz and G.F. Bertsch, Nucl. Phys. **A533** (1991) 712
55) G.F. Bertsch, Nucl. Phys. **A400** (1983) 221c
56) P.J. Siemens, Nucl. Phys. **A428** (1984) 189
57) G.F. Bertsch, G.E. Brown, V. Koch and B.A. Li, Nucl. Phys. **A490** (1988) 745
58) H.M. Xu, W.G. Lynch, P. Danielewicz and G.F. Bertsch, Phys. Rev. Lett. **65** (1990) 843
59) G. Papp and D.H.E. Gross, to be published (1992)
60) T.K. Nyak, T. Murakami, W.G. Lynch, K. Swartz, D.J. Fields, C.K. Gelbke, Y.D. Kim, J. Pochodzalla, M.B. Tsang, H.M. Xu, F. Zhu and K. Kwiatkowski, Phys. Rev. Lett. **62** (1989) 1021
61) T.K. Nyak, T. Murakami, W.G. Lynch, K. Swartz, D.J. Fields, C.K. Gelbke, Y.D. Kim, J. Pochodzalla, M.B. Tsang, H.M. Xu, F. Zhu and K. Kwiatkowski, Phys. Rev. **45** (1991) 132
62) F. Zhu, W.G. Lynch, D.R. Bowman, R.T. de Souza, C.K. Gelbke, Y.D. Kim, L. Phair, M.B. Tsang, C. Williams, H.M. Xu and J. Dinius, Phys. Lett. **B282** (1992) 299
63) J. Hubele, P. Kreutz, J.C. Adloff, M. Begemann-Blaich, P. Boissou, G. Imme, I. Iori, G.J. Kunde, S. Leray, V. Lindenstruth, Z. Liu, U. Lynen, R.J. Meijer, U. Milkau, A. Moroni, W.F. Müller, C. Ngô, C.A. Ogilvie, J. Pochodzalla, G. Raciti, G. Rudolph, H. Sann, A. Schüttauf, W. Seidel, L. Stuttge, W. Trautmann and A. Tucholski, Z. Phys. **A340** (1991) 263
64) J. Aichelin and H. Stöcker, Phys. Lett. **B163** (1985) 59
65) Y.D. Kim, R.T. de Souza, D.R. Bowman, N. Carlin, C. Gelbke, W.G. Gong and S. Pratt, Phys. Rev. **C45** (1992) 338;
Y.D. Kim, R.T. de Souza, C.K. Gelbke, W.G. Gong and S. Pratt, Phys. Rev. **C45** (1992) 387